Arctic, Antarctic and Alpine Research, Vol. 39, No. 1, 2007, pp. 152–164

Snow Cover Conditions in the Tibetan Plateau Observed during the Winter of 2003/2004

Kenichi Ueno#*
Kenji Tanaka†
Hiroyuki Tsutsui‡ *and*
Maoshan Li§

*Graduate School of Life and Environmental Sciences, University of Tsukuba, Tennoudai 1-1-1, Tsukuba Ibaraki, 305-8572, Japan.
†Department of Civil Engineering, Kumamoto University, Kurokami 2-39-1, Kumamoto, 860-8555, Japan.
‡Department of Civil Engineering, University of Tokyo, Bunkyo-ku, Tokyo, 113-8656, Japan.
§Cold and Arid Environment & Engineering Research Institute, Chinese Academy of Science, 260 Donggang West Road, Lanzhou 730000, China.
#Corresponding author.
kenueno@sakura.cc.tsukuba.ac.jp

Abstract

Surface conditions in the non-mountainous areas of the central Tibetan Plateau were measured in a field survey in February 2004, and water balance parameters such as precipitation, sublimation, and water equivalent of snow cover were examined through the 2003/2004 winter by *in situ* automated measurements. Snow cover was shallow and coexisted with snow-free areas, producing large surface temperature heterogeneity under strong insolation. Clear diurnal variation was found in the meteorological observation. The precipitation and total sublimation from November 2003 to January 2004 were estimated as 15 mm and 17 mm, respectively, and the remaining equivalent snow water quantity in the beginning of February 2004 was 8 mm. Imbalance of the water budget was mainly due to the uncertainty of snow cover proportion within the mesoscale area. Importance of a redistribution process of the snow was proposed to explain the consistency of surface heating and remaining snow cover.

Introduction

On the Tibetan Plateau, low temperature conditions due to high elevations, exceeding 4000 m a.s.l., allow snowfall at times even in the summer monsoon season. However, strong insolation prevails throughout the year due to the low latitude, which is favorable for the activation of energy and water cycles between the land and atmosphere. Such unique climate conditions—cryosphere in the lower latitudes—have attracted many scientists to investigate thermal effects on continental-scale climate variability (e.g., by Kuhle, 1987). The impact of plateau-scale snow cover to the successive Asian summer monsoon is an important question (Dey and Bhanu Kumar, 1982; Wu and Qian, 2003; Qian et al., 2004); albedo and snow-hydrological feedback of the excess snow mass are proposed as physical mechanisms (Yasunari et al., 1991). Most of the studies have used station- or grid-based objective analysis data distributed in a 100-km scale. The analyses have been conducted by statistical and diagnostic methods, or numerical simulations with many assumptions for surface boundary conditions. Recently, weekly satellite estimates of snow cover have been prepared to improve those boundary conditions and assess their year-to-year variation (e.g., Koike et al., 2001). The plateau has discontinuous or sporadic permafrost where complex topography causes surface heterogeneity by means of snow cover, vegetation, or soil moisture. Therefore, intensive *in situ* observational studies had been anticipated to reveal sub-grid-scale processes of land-atmosphere interactions.

GAME-Tibet project, a part of regional experiments of GEWEX (Global Energy and Water Cycle Experiment) Asian Monsoon Experiment (GAME; GAME International Science Panel, 1998), was one of the pioneer research activities to meet this task. The project introduced modern observational equipment, such as multiple automated weather and hydrology stations (AWS; Table 1) with a Doppler radar and flux turbulence measurement system, and conducted intensive observations for four successive months (from May to August); the undertaking covered a monsoon season in 1998 at Naqu basin (31°N, 92°E). For the snow cover issues, Takayabu et al. (2001) compared the land surface models with common forcing data observed at the Tanggula Mountain area (around 5000 m a.s.l.) and pointed out that estimation of water equivalent of snow (WES) was strongly affected by the treatment of albedo. If the heat budget was calculated without consideration of dividing bare-soil and snow cover areas, snow cover melted too much by the effects of bare soil. Unfortunately, GAME could not accomplish the investigation of snow cover effects in the non-monsoon periods in non-mountainous areas.

There are a limited number of studies over the plateau areas focused on land-atmosphere interaction during the winter season. From the global point of view, Murakami (1981) diagnosed the diurnal variations of winter atmospheric circulations around the plateau by using objective analysis data and indicated the deep penetration of the diabatic processes operating within the planetary boundary layer (PBL) with diurnal variation in the wind hodographs. For the *in situ* snow cover conditions, Sato (2001) conducted continuous automated measurements of snow depth and WES from 1993 to 1999 in the Naqu area, and revealed that snow depth was normally less than 10 cm, but sometimes lasted for over one month. Consequently, a simple question may arise concerning how such diurnal atmospheric circulation can exist with month-long continuous snow cover. In 2002, Co-ordinated Enhanced Observing Period (CEOP)/Asian Monsoon Project (CAMP; Koike, 2004) was launched. In the Tibetan Plateau, CAMP reconstructed the GAME-AWSs to CEOP-AWSs

1523-0430/07 $7.00

TABLE 1

List of principal abbreviations used in this paper.

AWS	Automated weather station
CEOP	Coordinated enhanced observing period
CMO	Chinese meteorological observatories
ESWQ	Equivalent snow water quantity
PBL	Planetary boundary layer
SCP	Snow cover proportion
WES	Water equivalent of snow

by introducing ground-based remote-sensing sensors, such as a wind profiler and intelligent radiation sensors, to conduct one-dimensional quantitative validation of satellite estimates and provide data for four-dimensional assimilation in the weather forecasts. The system was also improved to run for a year by using a solar-power generator system (Tanaka et al., 2003; Hirose and Koike, 2004).

In February 2004, the CEOP/CAMP/Tibet project conducted a preliminary winter expedition along the Tibet highway running north-south of the central plateau. The main target was to maintain the AWS system and observe the actual snow cover conditions. Based on field data obtained by this expedition, this paper reveals the characteristics of basic water budget components, such as precipitation, sublimation, and snow accumulation, during a core-winter season in the non-mountainous areas. Important functions of snow accumulation conditions for surface heating process are investigated. First, characteristics of winter weather and precipitation variability are described. Second, surface conditions and snow cover structures are introduced, and the aerial amount of WES is estimated. Third, sublimation amount was estimated by empirical and heat budget methods. In the summary, water balance among those components is examined, and possible mechanisms of snow redistribution processes to control the land-atmosphere interaction are discussed.

Observations and Data

This study focused on the period from November 2003 to April 2004, referred to as "winter 2003/2004." Several *in situ* data at Chinese meteorological observatories (CMO) in the plateau and station data at Kathmandu in H.M.G. Nepal were collected from the data archive at Daily Global Summary of Day (GLOBAL-SOD) Station Data, National Oceanic and Atmospheric Administration (NOAA). Daily precipitation data at Thimphu in Bhutan were also collected with personal communications. Location of the observatories is shown in Figure 1a and Table 2. Most of the CMO are located in urban areas where precipitation is manually measured, but snowfall and snow cover conditions may be strongly affected by these artificial conditions. The CEOP-AWSs are located in a flat natural area where there is no commercial power supply. Daily precipitation data at CMO ($\times$ marks in Fig. 1b) were used to determine precipitation events and amounts, while hourly snow-depth and radiation data at CEOP-AWSs ($\bullet$ marks in Fig. 1b) were used for determining snow cover periods and estimating the amount of snow. The planetary boundary layer (PBL) tower data at BJ and ANNI sites (Tanaka et al., 2003), located near the center of the Naqu basin (31.48°N, 92.06°E), were used for surface energy budget calculations. As a result, meteorological measurements used for this study differed depending on the site (Table 2). Snow depth was instantaneously measured by an ultrasonic snow-depth sensor with an accuracy of 1 cm. Albedo, a ratio of upward and downward short wave radiation, was measured with a 10 minute average. The radiation sensors were attached 2 m above the ground and could detect reflections from about 10 m of the surrounding surface. Both data were collected at hourly intervals.

During February 3–11, 2004, a winter survey was conducted along a 1200 km transect from Golmud to Lhasa City along 90–92°E and passing CMO stations 3–6 (Fig. 1a). During the survey, simple land-surface and meteorological observations were conducted at 23 points, including observations at the CEOP-AWSs. Among those points, snow cover existed at 19 points where the snow cover observation was carried out. Those points are named with an "S" with numbers starting from north to the south along the survey route (a detailed location map for those points are omitted, but the latitude/altitude information is shown at the top of Fig. 6). As the snow cover is often discontinuous, we determined an observation point by visual and multiple snow-depth measurements where the pattern of the discontinuity was initially representative. Then, snow temperature, stratigraphy, grain size, density, and WES were measured at several snow profiles. 1 mm $\times$ 1 mm mesh gauge and 50 cm^3 stainless steel cylinders were used for measurements of the snow grain diameter and density, respectively. Snow quality at each layer was classified using categories of the Japanese Society of Snow and Ice (1991). This classification is nearly the same as that of the International Association of Hydrological Sciences (IASH) and the International Commission on Snow and Ice (ICSI) working group on snow classification. Snow cover proportion (SCP), the percentage of snow cover in areas about 100 m $\times$ 100 m around the snow survey point, was visually determined, and an average snow depth in the snow cover areas was obtained from the 5 to 10 snow-depth measurements. This study determined a spatial equivalent snow water quantity (ESWQ) at each point by multiplying the SCP by WES measured at a representative snow profile.

Meteorological observations, such as measuring temperature, wind speed with direction, humidity, albedo, and ground surface temperature, were conducted at each point during the winter survey. When the location consisted of mixed surface types, such as snow cover, bare-soil, or grasslands, surface and multiple subsurface temperatures were measured by infrared radiation thermometer and digital temperature sensor.

Global reanalysis data of National Centers for Environmental Prediction (NCEP) and National Center for Atmospheric Research (NCAR) were used to analyze the atmospheric circulation patterns, and geostational meteorological satellite images of METEOSAT-5 provided by the EUMETSAT were used to analyze the cloud activities in cases of precipitation events.

Results

WINTER WEATHER AND PRECIPITATION

Variations of surface wind and air temperature during the winter season observed at the Tanggula mountain area (D105, 5040 m) and southern basin area (ANNI, 4480 m) are shown in Figure 2. Usually, wind speed at high elevations is strong through the day in the mid-latitude winter season due to the effects of synoptic-scale wind; however, evident diurnal changes of the wind speed, such as an increase of more than 10 m s^{-1} in the evening and a frequent calm condition in the late night, were observed in the plateau. Daily minimum air temperature was nearly the same at both stations, and it was sometimes below -20°C in January and February. On the other hand, daily maximum temperature differs between the stations by about 7°C for each 600 m of altitude difference, which is approximately equal to the dry

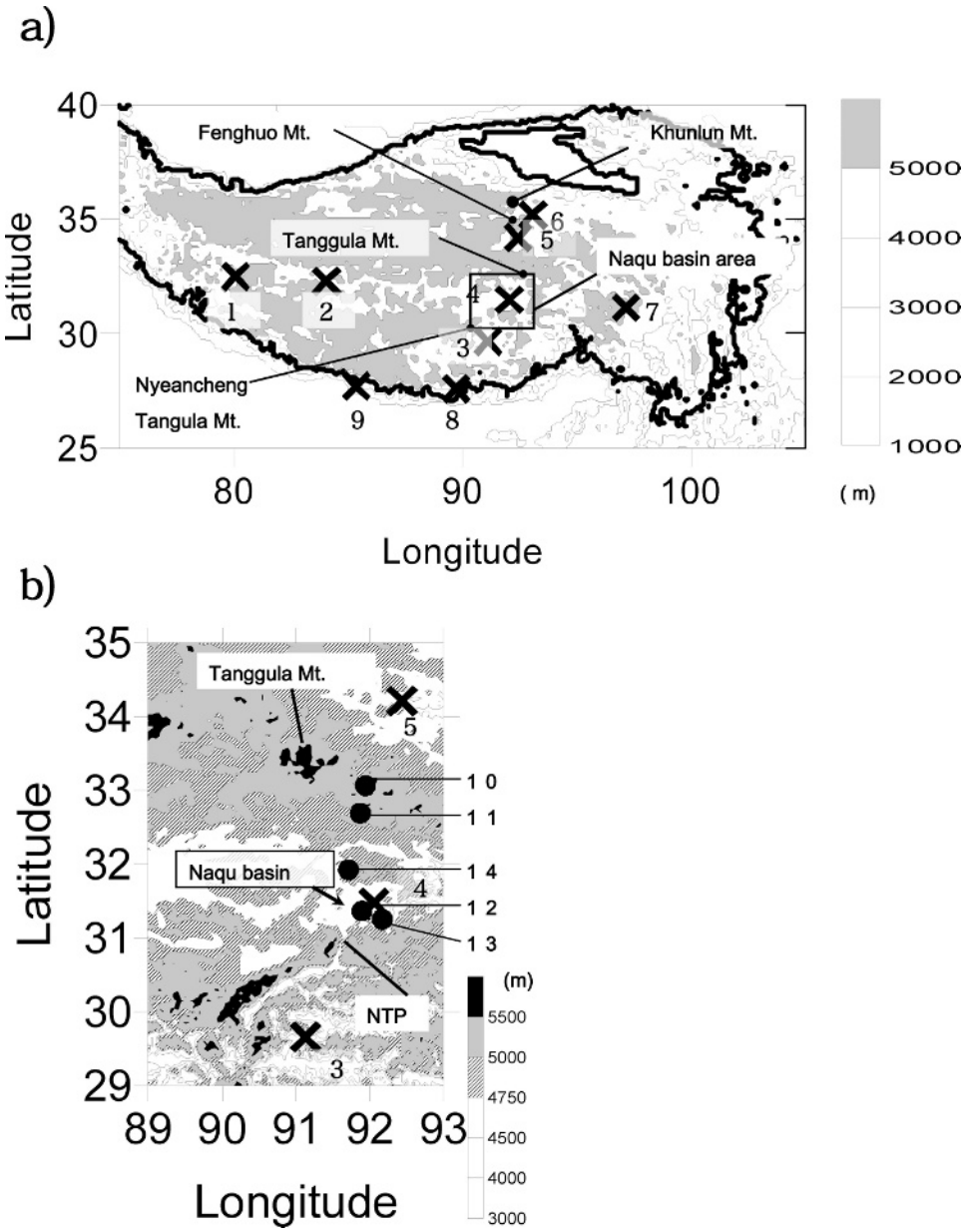

FIGURE 1. (a) Tibetan Plateau with locations of the Chinese meteorological observatories, Katmandu and Thimphu (×). (b) Naqu basin area (solid box in Fig. 1a) with locations of the CEOP-AWS (●). Numbers under the marks correspond to stations listed in Table 2. NTP = Nyeancheng Tangla Pass.

TABLE 2

Station list of CEOP-AWS and meteorological elements used for analysis.

Site number (Fig. 1)	Station name	Altitude (m)	Location (lat. N/long. E)	Elements*	Category**
1	Shequanhe	4279	32.50/80.08	Pr.	CMO
2	Gerze	4416	32.30/84.05	Pr.	CMO
3	Lhasa	3650	29.66/91.13	Pr.	CMO
4	Naqu	4508	31.48/92.06	Pr.	CMO
5	Tuotuohe (TUO)	4539	34.22/92.44	Pr.	CMO
6	Woudaoliang	4613	35.21/93.08	Pr.	CMO
7	Qamdo	3307	31.15/97.16	Pr.	CMO
8	Thimphu	2375	27.58/89.72	Pr.	PERS
9	Kathmandu	1337	27.70/85.36	Pr.	GLOB
10	D105	5039	33.06/91.94	AT, WS, Al, EB	CEOP
11	D110	4985	32.69/91.87	SD	CEOP
12	BJ	4509	31.37/91.90	SD, Al, EB	CEOP
13	ANNI	4480	31.25/92.17	AT, WS, SD, Al	CEOP

* Pr.: precipitation, AT: air temperature, WS: wind speed, SD: snow depth, EB: energy budget analysis, Al: albedo.

** CMO: Chinese meteorological observatories, GLOB: GLOBALSOD station, CEOP: CEOP-AWS, PERS: Personal exchange.

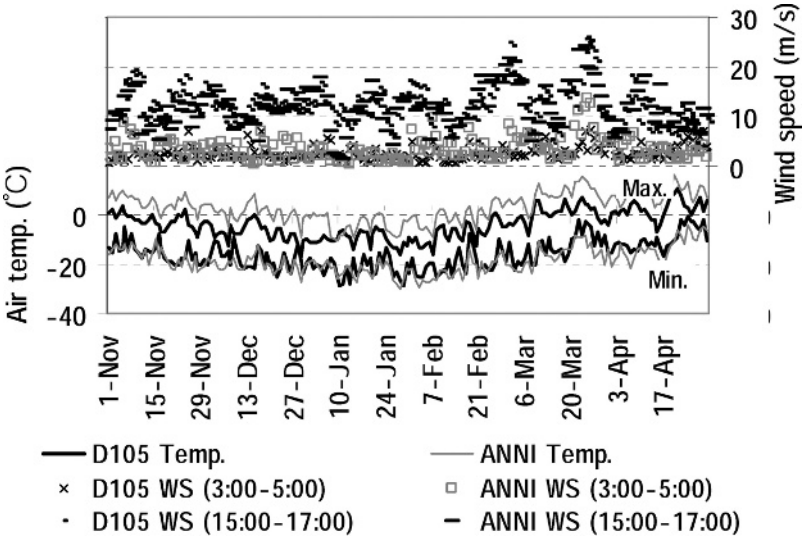

FIGURE 2. Average hourly wind speed at 5 m during the night (3:00–5:00) and evening (15:00–17:00), shown above; and maximum and minimum air temperature at 1 m, shown below, for D105 and ANNI stations, respectively.

adiabatic lapse rate. Average downward shortwave radiation during November 2003 to April 2004 at the two sites was 195 W m^{-2}, which is 70% of solar radiation estimated at the top of the atmosphere (283 W m^{-2}) and four times larger than the data observed at Yakhutsuku, Siberia (62.26°N, 129.62°E) in the winter 1998/1999 by Ohta et al. (2001). Thus, very strong insolation prevails in the winter plateau. Day-to-day variation of the insolation is compared between the morning and afternoon in Figure 3. The insolation during the afternoon was often lower than in the morning, indicating the diurnal development of clouds. To summarize these observations, diurnal development of the PBL with daytime cloud development prevailed under strong insolation even in the winter plateau. The phenomenon corresponded to the indications based on objective analysis by Murakami (1981). Additionally, Figure 3 shows decreasing insolation after late March, and monthly radiation in April became 30 W m^{-2} less than that in March. Fujinami and Yasunari (2001) showed that daily variation of the cloud activities has a peak in spring, prior to the pre-monsoon season, by using geostationary satellite images, which agreed with this *in situ* observational result.

Figure 4a shows mean seasonal precipitation for 10 years (1993–2004) at the stations in Figure 1a. Loss of solid precipitation in cases of strong wind is expected in the plateau (Ueno and Ohata, 1996); however, it is very difficult to correct the values because of the different environments of gauge installation at each observatory, so that correction is not carried out in the present study. Migration of western disturbance with the trough is explained as the major cause of winter precipitation around the Tibet/Himalaya regions (Lang and Barros, 2004; Ueno, 2005). In the Nepal Himalayas, tropical cyclones also cause heavy precipitation and avalanches in November and December (Yamada et al., 1996). Such sporadic increases of daily precipitation by tropical cyclones were found in Kathmandu precipitation data (results were omitted); however, the winter precipitation at stations on the plateau showed different features. Total precipitation during the non-monsoon season (October to May) is as small as 100 mm or less, and it is around 50 mm during the winter (November to April). The total amount did not always increase toward the west, and no sporadic heavy precipitation days associated with tropical cyclones were found. Moreover, precipitation days in the central plateau (e.g., Naqu) were the same or more than those in the Himalayas (e.g., Thimphu or Kathmandu) such that about 30 days of precipitation occurred during the winter.

Year-to-year variation of precipitation and days at Naqu observatory is shown in Figure 4b. Averaged annual non-monsoon (winter) amount was 111 mm (43 mm) with 59 (35) days, which corresponds to 1.3 mm d^{-1} of precipitation per week during the winter. Year-to-year variation of the winter amount is less than 20 mm, and the tendency of the variation was similar to that at Tuotuohe and Wudaoliang, which are located in the north of Naqu basin (Fig. 1a). Winter precipitation in 2003/2004 was normal. Heavy snow was reported in winter 1997/1998 in the Naqu basin (Xuezhan, 2001), but Figure 4b does not show the extreme increase of precipitation amount in the same winter. We speculate that precipitation frequency and accumulation condition

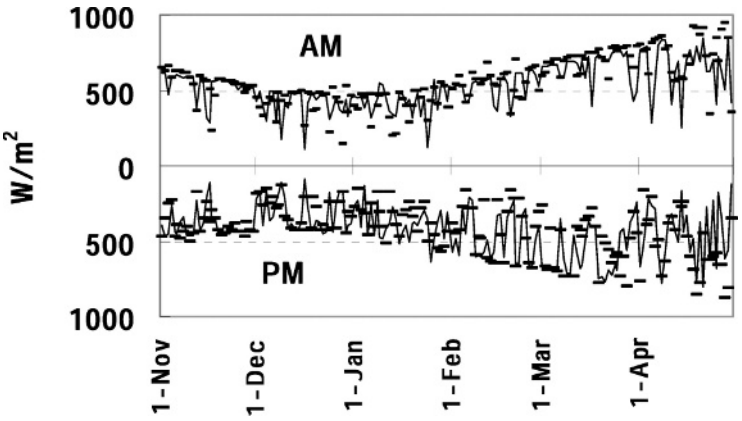

FIGURE 3. Downward shortwave radiation at ANNI (solid line) and D105 (dots) averaged for 8:00–10:00 (a.m.) and 13:00–15:00 (p.m.) local time.

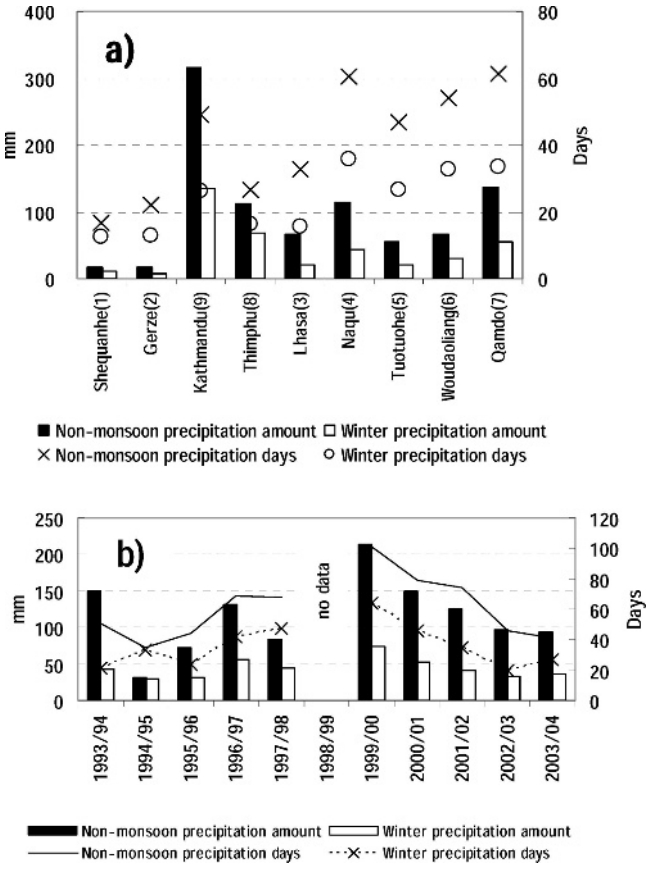

FIGURE 4. (a) Comparison of accumulated winter (November to April) and non-monsoon (October to May) precipitation amount and days at the stations in Figure 1a from 1993 to 2004 (except the data at Thimphu for 1993–1999). (b) Their year-to-year variation at Naqu CMO.

are important factors for the ''heavy snow'' and will discuss them in the final section.

Occurrence of snowfall and snow cover during the non-monsoon season was examined by daily albedo and snow-depth change (Fig. 5). Observation sites for these two elements are not always the same due to data acquisition problems. Daily albedo is the average value for 10:00–14:00 local standard time (LST). The albedo for the snow-free period is almost constant at 0.23 at any site; however, occurrence of snow cover induced abrupt changes in albedo and snow depth. Since the albedo on the continuous snow cover did not show large differences during mobile observation (see next section of text), the progressive decreases in albedo from high values associated with snowfall events (Fig. 5a) were due to changes of snow cover proportion within the sensor's footprint. Snow depth was shallow at AWS stations, such as the maximum of 14 cm at the BJ site. Frequent snow cover for short periods prevailed in the mountain areas, such as at D105, and it remained continuously for January and February in the southern basins, such as at BJ and ANNI. Appearance of plateau-scale snow cover may suppress the PBL development with weakening of surface wind in the daytime. The short-term appearance of snow cover sometimes corresponded with weakening of evening wind speed, but there is no month-long weakening of surface wind in Figure 2 corresponding to the January and February snow covers at BJ and ANNI. As will be described in the next section, distribution of snow cover is quite heterogeneous depending on the accumulation environment, and instruments and fences of the AWSs sometimes caused snow drifts and affected snow cover measurements. Therefore, the month-long continuous snow covers observed at BJ and ANNI may not represent the occurrence of large-scale continuous snow covers. Accordingly, significant information from the albedo and snow-depth data at AWS sites includes (1) snowfall days estimated from sudden increase of albedo, (2) snowfall amount estimated from increase of snow depth, and (3) sublimation amount estimated from the decreasing rate of snow depth with an assumption of density. Of those, (1) and (2) are presented in this section, and (3) is used in the section Sublimation and Heat Budget.

Precipitation events are defined by albedo, snow depth, and precipitation data. Each element has several observational problems. Albedo is missing during the night, and it is inaccurate during snowfall or cloudy weather. Snow-depth sensors cannot detect the exact time of snowfall in cases of weak intensity or blowing snow. The precipitation amount was manually measured only at CMO with daily bases. On the basis of comprehensive comparison of variability among those elements, we defined 16

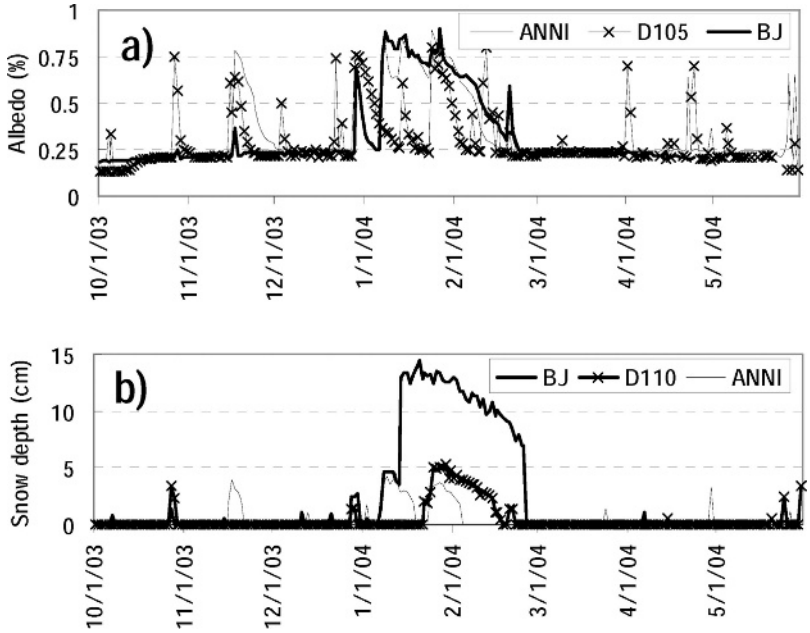

FIGURE 5. (a) Daily albedo, and (b) snow-depth change. Snow-depth data at BJ missing after April 24.

TABLE 3

Precipitation events from November 2003 to April 2004.

CASE	Period	Snowfall events estimated by albedo				Precipitation estimated by SD (mm)			Measured precip.(mm)		Synoptic condition		
		D105	D110	BJ	ANNI	D110	BJ	ANNI	TUO	NAQU	A	B	C
A	Nov. 15–18	*		*	*	0.0	0.0	7.9	0.5	1.3	¢	2	*
B	Dec. 2–3	*				0.0	0.0	0.0	0.0	0.0		3	¢
C	Dec. 27–28	*	*	*	*	2.1	0.0	3.1	2.0	1.6	*	4	
D	Jan. 2–3	*			*	0.0	0.0	3.6	0.3	0.0	*	2	
E	Jan. 6–9			*	*	0.0	5.3	4.0	0.0	5.6	*	1	¢
F	Jan. 12–15	*		*	*	0.0	10.9	0.0	0.5	3.5	¢	3(or 1)	*
G	Jan. 24–25	*	*		*	1.7	0.0	3.6	0.0	2.8	¢	1>3>2	*
H	Jan. 27			*	*	0.0	0.0	0.0	0.0	0.3	¢	1	¢
I	Feb. 1–2					0.0	0.0	0.0	0.5	0.0		2	*
J	Feb. 11–13	*				0.0	0.0	0.0	2.0	0.0	¢	2	
K	Feb. 19–20		no data	*	*	2.2	0.0	1.5	0.0	1.1	¢	1	
L	Apr. 3–5	*	nodata			0.0	0.0	0.0	0.0	3.1	¢	3	¢
M	Apr. 13–14		no data			2.7	1.5	0.0	2.0	4.0		2	¢
N	Apr. 21–22		no data		*	0.0	0.0	5.0	4.3	0.8	*	3	*
O	Apr. 24–26	*	no data			2.0	no data	4.0	0.5	9.8	*	4	¢
P	Apr. 29		no data			0.0	no data	4.0	0.0	2.8	*	3	
			Total @ Nov.-Jan.			3.8	16.2	22.2	3.3	15.1			
			Total @ Nov.-Apr.			10.7	—	36.7	12.6	36.7			

Synoptic condition: (A) trough at 500 and 200 hPa (*: apparent, ¢: weak); (B) synoptic cloud patterns by METEOSAT/IR (1: large-scale migration from west; 2: west-east zonal; 3: north-south zonal; 4: southwest-northeast zonal; 5: tropical cyclone); (C) pressure anomaly in East Asia at 500 and 200 hPa (*: apparent, ¢: weak; >: order).

cases of precipitation events that are summarized in Table 3. In many cases, occurrences of precipitation were also observed at Lhasa and Syangpoche station in the Nepal Himalayas, and were caused by plateau-scale disturbances as indicated by Ueno (2005). Total precipitation in each case was estimated from the increase of snow depth at D110, BJ, and ANNI sites with assumption of a new snow cover density of 0.1 g cm^{-3}. The amounts ranged from 2 to 10 mm per case, and the total amount for all cases almost corresponded to measured data of accumulated precipitation at CMO, such as 10 mm in the northern area (TUO) and 37 mm around the Naqu (bottom of Table 3).

Synoptic conditions were examined by pressure and water vapor vector distribution at NCEP 200 and 500 hPa fields, and METEOSAT-5 images. Regarding pressure fields, existence of a low-pressure trough over the southwestern plateau and a low-pressure anomaly in East Asia are evaluated as key synoptic factors (Ueno, 2005). Regarding satellite images, cloud shapes and migration patterns are classified into four types, and results are showed on the right side of Table 3. In most of the cases, a trough was identified at the southwestern part of the plateau. However, precipitation was sometimes caused without evident trough development during the core winter season. In such cases, a low-pressure anomaly over East Asia tended to prevail. Clouds had mostly not migrated from the west, but developed on the plateau with zonal structure. As the smaller precipitation amount in the western plateau (Fig. 4a) indicates, characteristics of winter precipitation in the central plateau are not explained simply by migration of a mid-latitude baroclinic trough; some unique thermodynamic mechanism may exist to cause a trough and bring water vapor into the central plateau.

SNOW-COVER CONDITIONS AND WATER EQUIVALET OF SNOW

This section describes the snow cover conditions observed by the snow survey during February 3–11, 2004. Most parts of the route are permafrost areas with bare soil, grasslands, or snow cover without trees or forests, and yak farming was frequently observed in the snow-free areas. The weather was almost fair, and it was calm in the morning and became windy in the afternoon, consistent with the results in Figure 2. There were light snow flurries when we passed the Fenghuo and Tanggula mountain ranges, but the snow blew away without any accumulation on the road. Snow depth, stratigraphy, SCP, and ESWQ at 19 sites are summarized in Figure 6. Density and grain size of each layer are also shown in Table 4. North of Khunlun Mountain range, a single layer of lightly compacted snow was distributed. According to the precipitation records at Tuo-tuo-he station (No. 5 in Fig. 1a), the layer probably formed during February 1–2. Snow cover was discontinuous at the kilometer scale in the Khunlun Mountain range, and was apparently controlled by differences in radiation intensity and drifting snow due to slope aspect and topographic undulations. Several meter-scale snow dunes formed in alignment with the prevailing wind direction in cases of flat continuous snow cover, which suggested the importance of the snow redistribution process to cause snow cover heterogeneity. South of the Khunlun mountain range, 2–3 layers were observed in the snow profile (Fig. 7a). According to Table 3, precipitation occurred during January 12–15, 24–25, and 27. Although we could not identify the exact date of accumulation in each layer, snow cover in the beginning of February apparently held the precipitation record from the middle of January. Snow cover disappeared between the Fenghuo Mountain and the Tanggula Mountain ranges. South of the Tanggula Mountain pass, such as at Naqu basin, snow-free areas coexisted with snow cover areas where the snow depth sometimes exceeded more than 50 cm.

Examples of discontinuous snow cover conditions are shown in Figure 8. Discontinuity within a 1-m scale, depending on the microtopography on the flat plains, was observed in the higher altitudes (Fig. 8a) or northern plain areas (Fig. 7b). The discontinuity was at a 10-m scale, oriented upslope-downslope in the southern Naqu basin at the lower altitudes (Fig. 8b). At

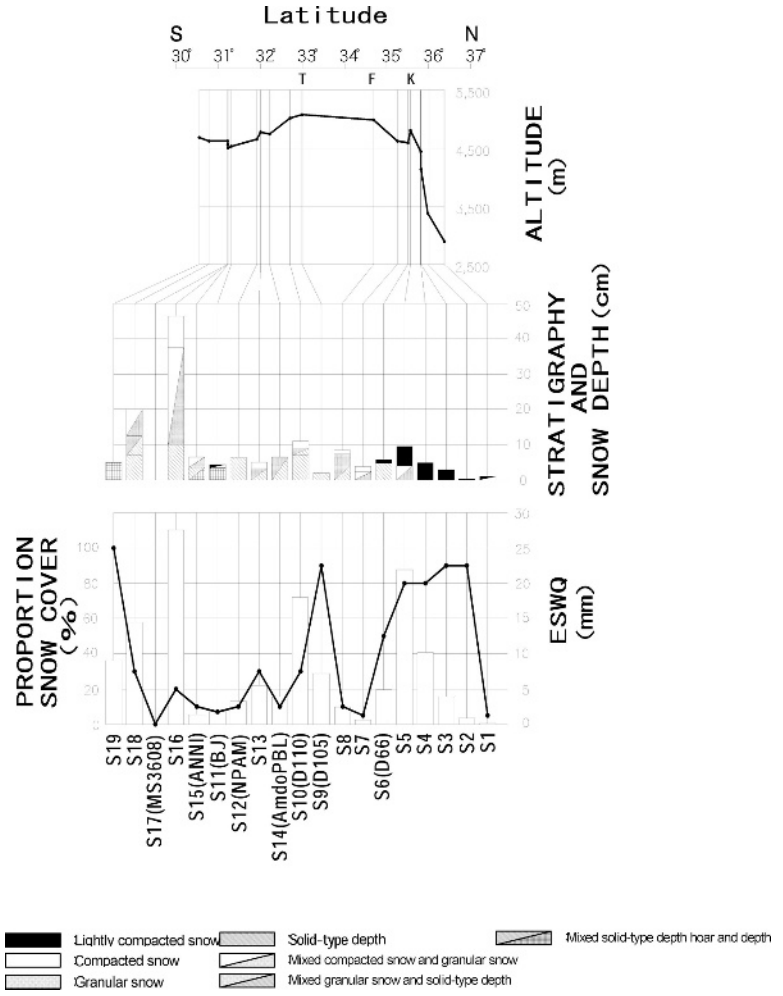

FIGURE 6. Stratigraphy, and SCP/ESWQ distribution at the snow survey points during February 3–11, 2004, with locations of altitudes. The solid line (solid bars) in the bottom figure corresponds to snow cover proportion (ESWQs).

present, snow cover proportion for these spatial scales is difficult to determine by remote sensing measurements. Therefore, we determined the proportion by ground observation. One unique characteristic of discontinuous snow cover was the shape of the sidewall. As shown in Figure 7b, overhanging snow covers on the snow-free ground were frequently observed during the trip. It is apparent that sidewalls were affected by strong radiation from the snow-free ground with high skin temperature. The depth hoar layers were sometimes observed indicated that a large vertical temperature gradient existed in the shallow snow layer. An example of the subsurface temperature distribution observed at Fenghuo Mountain pass (S8, 4960 m a.s.l.) is shown in Figure 9. Snow cover was 8.5 cm depth, composed of three layers divided at 7.3 cm and 4 cm from the ground surface, respectively. An earth hummock area was composed of convex-up topography (about 10 cm height and 20 cm width) with short grass. Although the air temperature was below -10°C, the ground surface temperature was above 0°C, and more than 10°C difference existed between earth hummocks and snow cover. Soil temperature at 5 cm showed similar differences. Thus, quite large surface thermal contrasts prevailed due to the coexisting thin snow cover and snow-free areas.

ESWQ ranged from 5 to 25 mm (Fig. 6), with an average of 8 mm. Compared with the total precipitation after November 2003 (about 15 mm; see bottom of Table 3), half of the precipitation had remained at the beginning of February 2004. SCP tended to increase in the mountainous regions, such as around Khunlun, Tanggula, and Nyeancheng Tangla pass; however, individual relations of ESWQ vs. SCP and ESWQ vs. snow depth were not so clear. The cause of the ESWQ variation was examined at specific sites, such as at S5, S10, S16, and S19 (Table 5). At S5, the major factors contributing to a large ESWQ were high SCP, less radiation on a north-facing slope, and complex topography that reduced the wind. At S10, abnormally large snow density caused high ESWQ. The site was flat and exposed to prevailing winds at the southern foot of the Tanggula Mountains, where light snow does not readily accumulate. At S16, the large snow depth increased the ESWQ. The site was facing east, leeward of the prevailing wind, and it was apparently affected by snowdrift. ESWQ was small at S19, even though the SCP was 100%; the snow depth was 5 cm with a density of 0.18 g cm^{-3}. The site was located at the bottom of a deep valley in the Nyeancheng Tangula Mountain ranges, where development of depth-hoar caused the small density. Spatial variability of the ESWQ amount is not determined by a unique factor, and accumulation environments of the shallow dry snowfall are primarily important to determine the spatial variability of ESWQ.

Redistribution of snow cover is one of the important processes to consider both for water budget estimation and for hydro-meteorological observation technique. Figure 10 is an example of snowdrifts around the AWS at BJ site. Clear snowdrifts deposited in the leeward of the AWS site were observed, affected by housing, precipitation gauge, and fence. Maximum snow depth exceeded more than 50 cm. During the expedition, such snowdrifts were also found at Amdo, D110, and ANNI AWS sites. At most of the stations, the drifted snow

TABLE 4

Density and grain size of each layer at stations in Figure 6.

Station number (lat. N/long. E)		Density (g cm^{-3})	Grrain size (mm)
S1 (36°20′50″/94°49′53″)	Upper layer	—	—
	Middle layer	—	—
	Bottom layer	0.30	0.60
S2 (35°55′41″/94°48′26″)	Upper layer	—	—
	Middle layer	—	—
	Bottom layer	0.33	0.30
S3 (35°44′32″/94°17′52″)	Upper layer	—	—
	Middle layer	—	—
	Bottom layer	0.15	0.18
S4 (35°44′01″/94°13′09″)	Upper layer	—	—
	Middle layer	—	—
	Bottom layer	0.26	0.13
S5 (35°33′58″/93°58′21″)	Upper layer	—	—
	Middle layer	0.28	0.20
	Bottom layer	0.30	0.50
S6(D66) (35°31′29″/93°47′05″)	Upper layer	—	—
	Middle layer	0.30	0.30
	Bottom layer	0.25	2.10
S7 (35°17′11″/93°14′45″)	Upper layer	—	—
	Middle layer	0.35	0.75
	Bottom layer	0.30	2.50
S8 (34°40′45″/92°54′58″)	Upper layer	0.30	0.75
	Middle layer	0.30	1.75
	Bottom layer	0.28	2.00
S9 (D105) (33°03′52″/91°56′33″)	Upper layer	—	—
	Middle layer	—	—
	Bottom layer	0.40	3.25
S10 (D110) (32°41′38″/91°52′13″)	Upper layer	0.55	0.75
	Middle layer	0.70	2.25
	Bottom layer	0.50	3.00
S14 (AmdoPBL) (32°14′29″/91°37′27″)	Upper layer	—	—
	Middle layer	—	—
	Bottom layer	0.30	2.00
S13 (32°01′27″/91°41′40″)	Upper layer	—	—
	Middle layer	0.40	0.55
	Bottom layer	0.35	2.25
S12 (NPAM) (31°55′28″/91°42′52″)	Upper layer	—	—
	Middle layer	—	—
	Bottom layer	0.28	3.50
S11 (BJ) (31°22′09″/91°53′55″)	Upper layer	—	—
	Middle layer	0.37	0.61
	Bottom layer	0.31	4.56
S15 (ANNI) (31°15′17″/92°10′23″)	Upper layer	—	—
	Middle layer	0.32	1.25
	Bottom layer	0.30	4.00
S16 (31°15′34″/92°07′00″)	Upper layer	0.28	0.65
	Middle layer	0.30	1.25
	Bottom layer	0.30	2.50
S18 (30°45′34″/91°35′08″)	Upper layer	0.24	1.25
	Middle layer	0.30	2.25
	Bottom layer	0.28	3.75
S19 (30°35′47″/91°30′15″)	Upper layer	—	—
	Middle layer	—	—
	Bottom layer	0.18	4.75

affected the footprint of the upward radiation sensor, and point-measured snow-depth data were also indirectly affected. Heat budget analysis of AWS data was conducted by taking into account those conditions in the next section.

SUBLIMATION AND HEAT BUDGET

During December to February, air temperature was almost always below 0°C (Fig. 2), and refrozen melt layers were not observed in the snow profiles during snow survey. Therefore, the decrease in ESWQ during winter was expected mostly due to sublimation at the snow cover surface. This study estimated the sublimation amount by two methods: (A) an experimental method using the trend of decreasing snow depth, and (B) a heat budget method to estimate latent heat. Method (A) estimates the sublimation from the snow cover areas, while method (B) estimates the spatial averaged sublimation including snow-free areas in the footprint of the AWS. For method (A), WES was

FIGURE 7. Snow layer observed at (a) S5 point, and (b) S6 point. S6 point is the same location as D66 CEOP-AWS site. Snow depths are 10 cm and 5 cm, respectively.

defined as:

$$\mathrm{WES} = D \times \rho, \tag{1}$$

where D equals snow depth and ρ equals snow density. If the SCP around the snow-depth sensor could be estimated from the albedo changes, daytime ESWQ around the AWS could be estimated by

$$\mathrm{ESWQ} = D \times \rho \times \mathrm{SCP}. \tag{2}$$

The experimental relation between albedo and SCP (Fig. 11), determined by the multiple observation during the snow survey trip, was used to estimate the SCP around the AWS from automated measurements of albedo (α). In Figure 11, the crosses

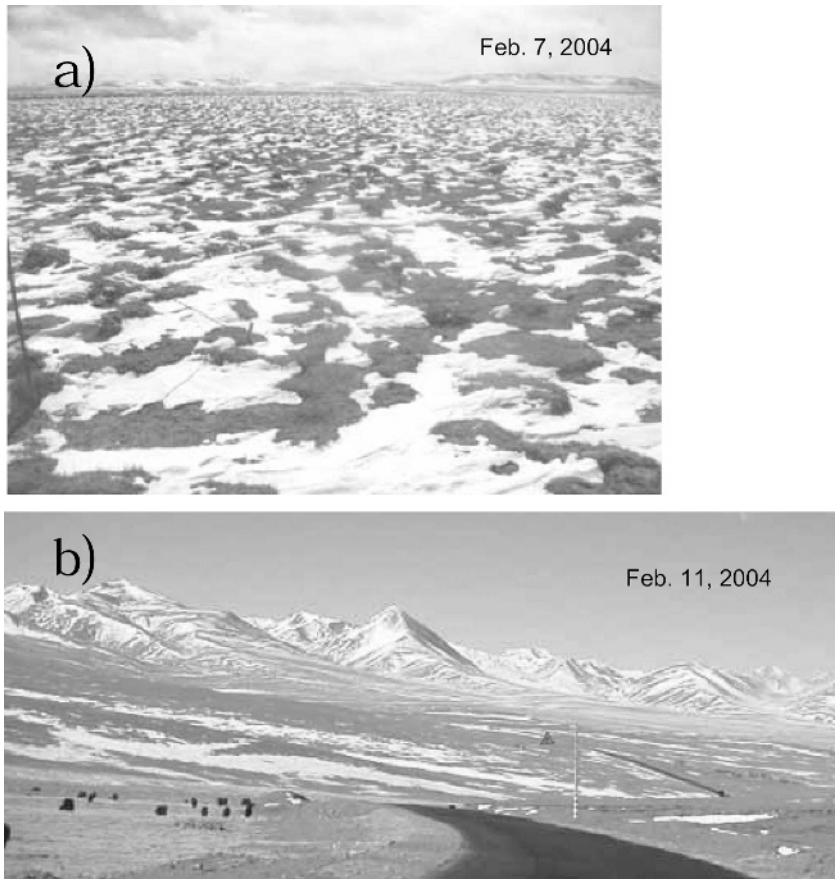

FIGURE 8. Surface condition at (a) S10 point and (b) south of Naqu City (near S15 point). S10 is the same location as D110 CEOP-AWS. Black spots in the lower left of (b) are yaks.

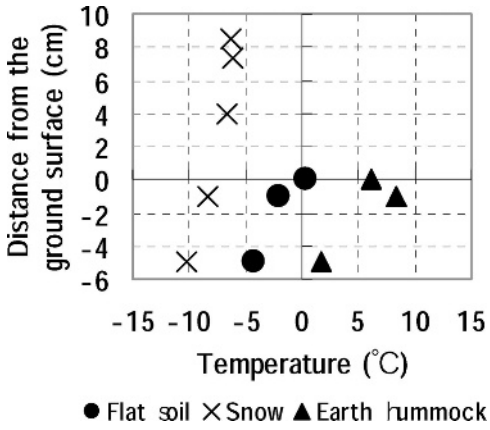

FIGURE 9. Comparison of temperature profiles with different surface conditions at Fenghuo Mountain pass on February 6, 2004, at 13:00 p.m. Air temperature at 1.5 m was −12.0°C with cloudy weather.

FIGURE 10. Snow cover trapped by the instruments and fence at the BJ site, in WSW direction.

indicate the underestimating of albedo measured in the valley because of the reflections from the snow covered slope. Except for those values, relations between α and SCP fit a linear function as follows:

$$\mathrm{SCP} = (2.86 \times \alpha) - 71.5\%; \tag{3}$$

SCP = 100% when $\alpha > 60\%$, and SCP = 0% when $\alpha < 25\%$. Albedo of snow-free areas became 25%, which agrees with the result of Figure 5a, and it did not differ between bare soil and grass areas. In the snow survey, average ρ in each profile did not vary significantly (Table 4), so ρ was treated as a constant value of 0.32 g cm^{-3}. Figure 12 shows calculated intraseasonal changes of ESWQ at BJ and ANNI. Due to snowdrifts at both sites, estimations of the remaining snow cover were affected by the construction of the AWS site. ESWQ showed linear declining trends during the snow cover periods, such as 0.38 mm d^{-1} for January 21–27 at BJ. For the ANNI site, it became 1.8 mm d^{-1} for November 18–21, 0.99 mm d^{-1} for January 11–18, and 0.72 mm d^{-1} for January 26 to February 3. When the assumed snow density was varied by ±10%, the slope of the trend varied by 0.82–1.13 times at BJ and 0.82–1.10 times at ANNI. However, the decreasing rate was abruptly increased at the BJ site after the AWS maintenance work was conducted on February 10. The decreasing rate became 1.92 mm d^{-1} for February 11–19, which is 5 times larger than for the previous period. The maintenance work made many spots in the snow cover around the AWS. We speculate that such artificial spots enhanced the radiation effects by increasing discontinuity of snow cover and accelerating the decrease of ESWQ. In other words, the decreasing rate of ESWQ was strongly related to the snow distribution patterns. For example, even with the same SCP, ESWQ will decrease faster if the snow cover is more patchy. Strong insolation in the plateau will enhance this process more compared to other parts of the cryosphere located in the northern latitudes.

Next, we applied method (B), the heat budget, at two CEOP-AWSs, the D105 site representing mountainous high elevation areas and the BJ site representing plains in the Naqu basin. Sensible (H) and latent heat (lE) flux were calculated based on the Bowen-ratio method by using differences in temperature and humidity observed at 8.2 m and 1.0 m from the ground. H and lE could be derived when the net-radiation (Rn) and soil heat flux (G) were given as follows:

$$lE = Rn - G(1 + \beta)^{-1} \tag{4}$$

$$H = Rn - G - lE \tag{5}$$

where β is the Bowen-ratio, defined as

$$\beta = C_p(T_1 - T_2)\, l(q_1 - q_2)^{-1} \tag{6}$$

Cp is the specific heat at a constant pressure (1005 J kg^{-1} K^{-1}), and l corresponds to latent heat of 2.50×10^6 J kg^{-1} for evaporation and 2.83×10^6 in J kg^{-1} for sublimation. Evaporation or sublimation was determined using the air

TABLE 5

ESWQ, Snow depth, SCP, and average density at S5, S10, S16, and S19 snow survey points, as shown in Figure 6. See Table 1 for explanation of abbreviations.

Unit	ESWQ (mm)	Snow depth (cm)	SCP (%)	Density (g cm^{-3})
S5	22.0	9.5	80	0.29
S10	19.1	11.0	30	0.58
S16	28.1	46.5	20	0.29
S19	10.0	5.0	100	0.18

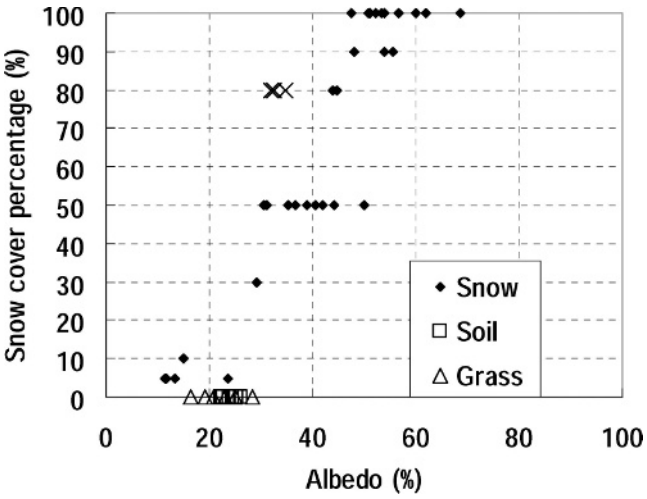

FIGURE 11. Relationship between albedo and snow cover percentage. Crosses indicate observation points located in the bottom of the valley with snow covered slopes.

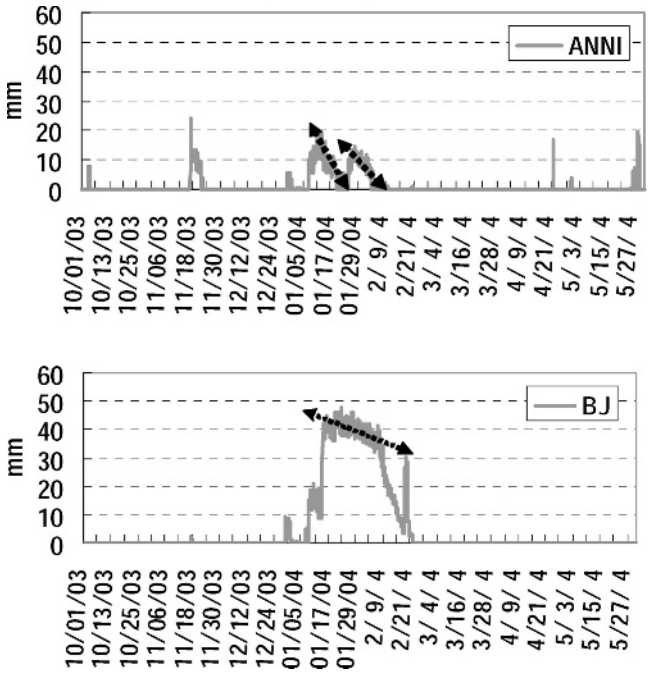

FIGURE 12. Time sequences of the equivalent snow water quantity at ANNI and BJ sites estimated by snow depth, albedo, and relation between albedo and snow cover percentage (Fig. 11). Arrows show the decreasing trends used to determine the sublimation.

temperature at 1 m above the ground. Temperature difference is directly calculated from the voltage difference of thermocouples at the two elevations. At the BJ site, soil heat flux was evaluated by the measurements at three small AWSs located 400 m from the main tower to avoid the snow drift around the tower.

Figure 13 shows the intraseasonal change of daily average surface heat budget at BJ site. Mostly, H was being balanced with Rn, indicating that sensible heat flux was dominant during winter. H and Rn gradually decreased until the middle of February, and then they recovered quickly in March and reached the same level as in the beginning of October. The lE gradually decreased after the middle of October and dropped below 10 W m^{-2} after the end of October; however, sharp increases in lE were found on November 17; January 7, 13–25, and 30–31; February 13 and 28; and March 12 and 23–27. Most of these cases corresponded with precipitation cases in Table 3. In particular, the period for January 13–25 overlapped the first half of a long-term snow covered period as shown in Figure 12. Hence, increases of latent heat flux qualitatively corresponded to the occurrence of snow at the AWS site. Suppression of H due to increase of SCP could increase the lE through the heat balance. Due to cloud development in March (Fig. 3), seasonal increase of Rn slowed down and suppressed the sensible heat; however, the latent heat did not increase, indicating that precipitation did not occur.

The rate of sublimation in water equivalent was calculated from the daily latent heat at D105 and BJ sites (Fig. 14). Sublimation of 1 mm d^{-1} corresponds to 32.8 W m^{-2} of daily latent heat flux. Decrease of daily sublimation due to decrease of lE was evident after October. During the winter in the dry climate condition, sublimation was less than 0.1 mm d^{-1}, and negative values were sometimes recorded. In snow covered periods, sublimation increased and exceeded 0.5 mm d^{-1} at the BJ site. Three months' average sublimation, from November 2003 to January 2004, was 0.04 mm d^{-1} at D105 and 0.18 mm d^{-1} at BJ. The total sublimation over the winter was 17 mm at the BJ site, approximately equal to the total precipitation (15 mm) and twice the remaining ESWQ (7 mm). Causes of the imbalance of those values are discussed in the next section. The daily average sublimation amount during the snow cover period for January 13–25 became 0.43 mm d^{-1}. The value is slightly (13%) larger but nearly equal to that estimated by the experimental method (0.38 mm d^{-1}). We concluded that the sublimation amount from the locally accumulated snow surface was about 0.4 mm d^{-1} during the core winter season.

Summary and Discussion

This paper describes the basic snow cover conditions during winter season in the central Tibetan Plateau based on the analysis of *in situ* data. In particular, the balance among precipitation, water equivalent of snow cover, and sublimation and factors that control their variation were examined.

CEOP-AWS network provided evidence of diurnal change of PBL with afternoon cloud development through the winter season; investigation of snow cover conditions was proposed to explain the processes to cause such surface heating. Winter precipitation amount and days in the central plateau were grater than in the western plateau, and not all precipitation events in the winter 2003/2004 were associated with synoptic cloud systems intruding from the west. This evidence suggested the necessity of further investigation for instability and moisture transportation to cause winter precipitation in the central plateau. In the Naqu area, the total precipitation amount during 2003/2004 winter (November–April) was about 40 mm (a normal year), provided by at least 16 precipitation events.

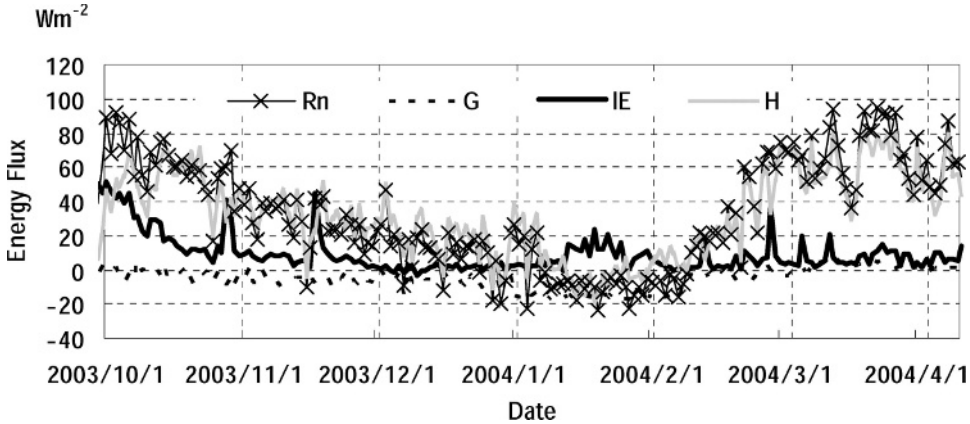

FIGURE 13. Daily average of surface energy fluxes at BJ site calculated by Bowen ratio methods.

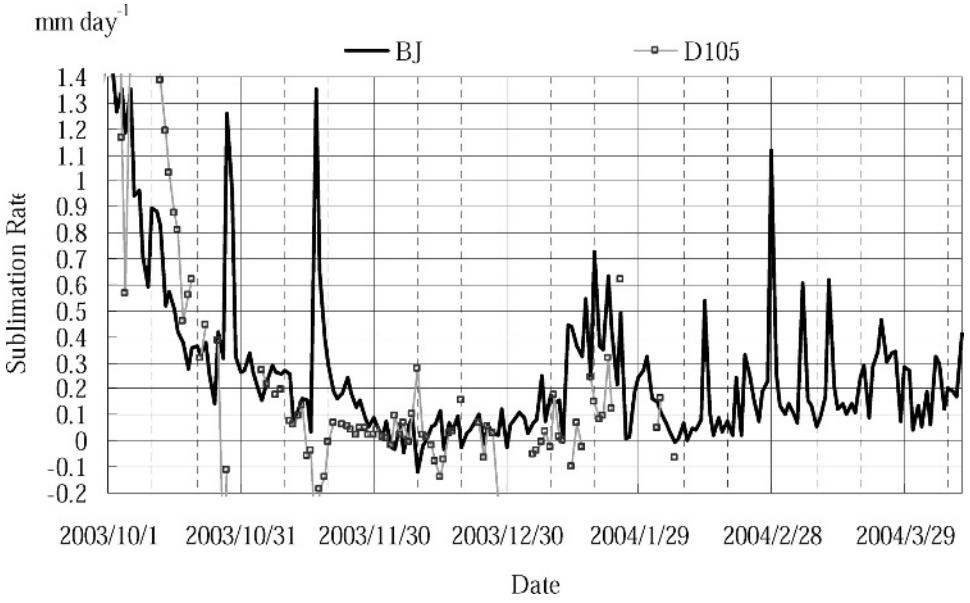

FIGURE 14. Daily equivalent sublimation rate estimated by latent heat flux at BJ and D105 sites.

Field observation in the beginning of February 2004 revealed that snow cover less than 10–20 cm depth coexisted with snow-free areas in patchy distribution. Large surface temperature heterogeneity occurred during the daytime due to the discontinuity of snow cover and vegetation distribution. Multiple layers were found in areas of shallow snow cover, representing precipitation records from the previous month. Snow layer deformation affected by the surface radiation and snow drifting was frequently observed during the expedition. Increase of ESWQ was not uniquely determined with snow depth or snow cover percentage. Moreover, local climate defining conditions of snow accumulation and redistribution was the major factor causing the spatial variability of ESWQ.

Sublimation of snow cover, estimated from the thinning rate of point-measured snow depth at the AWSs, varied from 0.4 to 1.8 mm d^{-1} depending on the snow cover periods and locations. We attributed the cause of variability to the difference in discontinuity patterns of snow covers. The daily average sublimation amount estimated by the Bowen ratio method was 0.18 mm d^{-1} at the BJ site from November 2003 to January 2004. The estimated sublimation rate during a major continuous snow cover period, January 13–25, was almost the same, around 0.4 mm d^{-1} between the experimental and heat balance methods.

During November 2003 to January 2003, total precipitation was 15 mm, sublimation amount estimated by the heat budget method was 17 mm, and the remaining equivalent snow water quantity (ESWQ) was 8 mm in the Naqu basin. The order of the water balance was almost consistent, so that the total precipitation amount was almost the same as that of sublimation, and ESWQ was almost half of the entire precipitation (sublimation). Imbalance of the budget was mainly due to uncertainty of the SCP. The SCP is a crucial factor for estimating both in-area average flux and ESWQ. The fact is, however, that there still remain large discrepancies among eye observation, albedo information, satellite estimation, and actual percentages at different scales.

Snow drifts found around the AWS raised a severe problem for automatic observation techniques. To explain the consistency among the characteristics of winter weather and snow cover characteristics as mentioned before, the snow redistribution process will be one of the important functions. Redistribution of the limited snowfall creates favorable conditions both for retaining snow for many weeks, where it accumulates, and for causing atmospheric heating over the snow-free areas, where it is removed. We expect that ''heavy snow'' is caused not only by the larger amount of snowfall, but also by the continuous snow covers over wide areas. This is only an initial study focused on the winter surface condition in the Tibetan Plateau. Intensive observation with longer monitoring of *in situ* data during the non-monsoon season, including a heavy snowfall year, is awaited.

Acknowledgments

This study was conducted as a part of the CEOP/CAMP/Tibet project supported by Core Research for Environmental Science and Technology of the Japan Science and Technology Agency, and by the Chinese Academy of Science. The authors are deeply grateful to Dr. Koike (Tokyo University), who implemented the winter expedition within the project, and to Mr. Sun and Mr. Yu (CARRERI) for assistance with the meteorological observations during the field experiments. Special thanks are also extended to Dr. S. Anderson and anonymous reviewers who gave us fruitful comments to improve the contents, and Dr. N. Naito (Hiroshima Institute of Technology), who provided the precipitation data at Thimphu, Bhutan.

References Cited

Dey, B., and Bhanu Kumar, O. S. R. U., 1982: An apparent relationship between Eurasian spring snow cover and the advance period of the Indian summer monsoon, *Journal of Applied Meteorology*, 21: 1929–1932.

Fujinami, H., and Yasunari, T., 2001: The seasonal and intraseasonal variability of diurnal cloud activity over the Tibetan Plateau: *Journal of the Meteorological Society of Japan*, 79: 1207–1227.

GAME International Science Panel, 1998: GEWEX Asian Monsoon Experiment (GAME) Implementation Plan, 136 pp.

Hirose, N., and Koike, T., 2004: Validation of the process for generating soil moisture distribution in the Tibetan Plateau. *In* Proceeding of the 6th International Study Conference on GEWEX in Asia and GAME: Kyoto, Japan.

Japanese Society of Snow and Ice, 1991, *Snow ice dictionary*. Kokonsyoin, Japan: 156 pp. (in Japanese).

Koike, T., 2004: The coordinated enhanced observing period, an initial step for integrated global water cycle observation. *WMO Bulletin*, 53(2): 2–8.

Koike, T., Fujii, H., Ohta, T., and Togashi, E., 2001: Development and validation of TMI algorithms for soil moisture and snow. *IAHS Publication*, 267: 390–393.

Kuhle, M., 1987: Subtropical mountain- and highland-glaciation as Ice Age triggers and the warming of the glacial period in the Pleistocene. *GeoJournal*, 14.4: 393–421.

Lang, T., and Barros, A. P., 2004: Winter storm in the central Himalayas. *Journal of the Meteorological Society of Japan*, 82: 829–844.

Murakami, T., 1981: Orographic influence of the Tibetan Plateau on the Asiatic winter monsoon circulation, Part 1. Large-scale aspects. *Journal of the Meteorological Society of Japan*, 59: 66–84.

Ohta, T., Hiyama, T., Tanaka, H., Kuwada, T., Maximov, T. C., Ohata, T., and Fukushima, Y., 2001: Seasonal variation in the energy and water exchanges above and below a larch forest in Eastern Siberia. *Hydrological Processes*, 15: 1459–1476.

Qian, Y., Zhang, Y., Huang, Y., Huan, Y., and Yao, Y., 2004: The effects of the thermal anomalies over the Tibetan Plateau and its vicinities on climate variability in China. *Advances in Atmospheric Sciences*, 21: 369–381.

Sato, T., 2001: Spatial and temporal variations of frozen ground and snow cover in the eastern part of the Tibetan Plateau. *Journal of the Meteorological Society of Japan*, 79: 519–534.

Takayabu, I., Takata, K., Yamazaki, T., Ueno, K., Yabuki, H., and Haginoya, S., 2001: Comparison of the four land surface models driven by a common forcing data prepared from GAME/Tibet POP'97 products. *Journal of the Meteorological Society of Japan*, 79: 535–554.

Tanaka, K., Tamagawa, I., Ishikawa, H., Ma, Y. M., and Hu, Z. Y., 2003: Surface energy budget and closure of the eastern Tibetan Plateau during the GAME-Tibet IOP 1998, *Journal of Hydrology*, 283: 169–183.

Ueno, K., 2005: Synoptic conditions causing nonmonsoon snowfalls in the Tibetan Plateau. *Geophysical Research Letters*, 32: DOI 10.1029/2004GL021421.

Ueno, K., and Ohata, T., 1996: The importance of the correction of precipitation measurements on the Tibetan Plateau. *Journal of the Meteorological Society of Japan*, 74: 211–220.

Wu, T., and Qian, Z. A., 2003: The relationship between the Tibetan winter snow and the Asian summer monsoon and rainfall: an observational investigation. *Journal of Climate*, 16: 2038–2051.

Xuezhan, C., 2001: The influence of abnormal snow cover over Qinhai-xizang plateau and East Asian monsoon on early rainy season rainfall over South China. *Quarterly Journal of Applied Meteorology*, 21: 358–367 (in Chinese).

Yamada, T., Fushimi, H., Aryal, R., Kadota, T., Fujita, K., Seko, K., and Yasunari, T., 1996: Report on the avalanche in Panga. *Seppyo*, 58: 145–155 (in Japanese).

Yasunari, T., Kitoh, A., and Tokioka, T., 1991: Local and remote responses to excessive snow mass over Eurasia appearing in the Northern spring and summer climate. *Journal of the Meteorological Society of Japan*, 69: 473–487.

Ms accepted June 2006